

NEUTRAL CARBON EMISSION IN LUMINOUS INFRARED GALAXIES THE [C I] LINES AS TOTAL MOLECULAR GAS TRACERS*

QIAN JIAO^{1,2,3}, YINGHE ZHAO^{4,5,6,7}, MING ZHU^{1,2}, NANYAO LU^{8,1}, YU GAO^{7,9} AND ZHI-YU ZHANG^{10,11}

Draft version September 5, 2018

ABSTRACT

We present a statistical study on the [C I] ($^3P_1 \rightarrow ^3P_0$), [C I] ($^3P_2 \rightarrow ^3P_1$) lines (hereafter [C I] (1–0) and [C I] (2–1), respectively) and the CO (1–0) line for a sample of (ultra)luminous infrared galaxies [(U)LIRGs]. We explore the correlations between the luminosities of CO (1–0) and [C I] lines, and find that $L'_{CO(1-0)}$ correlates almost linearly with both $L'_{[C I](1-0)}$ and $L'_{[C I](2-1)}$, suggesting that [C I] lines can trace total molecular gas mass at least for (U)LIRGs. We also investigate the dependence of $L'_{[C I](1-0)}/L'_{CO(1-0)}$, $L'_{[C I](2-1)}/L'_{CO(1-0)}$ and $L'_{[C I](2-1)}/L'_{[C I](1-0)}$ on the far-infrared color of 60-to-100 μm , and find non-correlation, a weak correlation and a modest correlation, respectively. Under the assumption that these two carbon transitions are optically thin, we further calculate the [C I] line excitation temperatures, atomic carbon masses, and the mean [C I] line flux-to-H₂ mass conversion factors for our sample. The resulting H₂ masses using these [C I]-based conversion factors roughly agree with those derived from $L'_{CO(1-0)}$ and CO-to-H₂ conversion factor.

Keywords: ISM: atoms — ISM: molecules — galaxies: starburst — submillimeter: galaxies

1. INTRODUCTION

Carbon monoxide (CO) is the most commonly used molecular gas mass tracer in galaxies (e.g. Solomon & Vanden Bout 2005; Bolatto et al. 2013). The low- J CO transitions trace the total molecular gas mass with the CO-to-H₂ conversion factor (X_{CO}). However, X_{CO} could vary by a factor of ~ 10 under different physical environments (e.g., Papadopoulos et al. 2012; Bolatto et al. 2013). Furthermore, low- J CO transitions in high- z galaxies become difficult to observe with currently available ground facilities due to their limited sensitivities and the increasing Cosmic Microwave Background (e.g., Zhang et al. 2016). The high- J CO transitions, on the other hand, can not trace the total molecular gas mass due to their high critical densities and excitation energies. Therefore, it becomes important and urgent to have

some alternative H₂ tracers when more and more high- z targets are routinely observed in high- J CO transitions (e.g., Carilli & Walter 2013).

The emission of the two fine-structure transitions of the atomic carbon (C I) in its ground state may be a particularly powerful molecular gas tracer besides canonical CO-based methods (e.g., Papadopoulos et al. 2004; Walter et al. 2011) due to the following reasons. The critical densities (n_{crit}) of [C I] ($^3P_1 \rightarrow ^3P_0$) (rest frequency: 492.161 GHz, hereafter [C I] (1–0)), and [C I] ($^3P_2 \rightarrow ^3P_1$) (rest frequency: 809.344 GHz, hereafter [C I] (2–1)) are $\sim 500 \text{ cm}^{-3}$ and $\sim 10^3 \text{ cm}^{-3}$ (Papadopoulos et al. 2004), respectively, which are similar to that of CO ($J = 1 \rightarrow 0$) (hereafter CO (1–0); $n_{\text{crit}} \sim 4.4 \times 10^2 \text{ cm}^{-3}$ at kinetic temperature $T_{\text{kin}} = 20 \text{ K}$; Yang et al. 2010). In classical photodissociation region (PDR) models, [C I] only exists in a narrow [C II]/[C I]/CO transition zone (Tielens & Hollenbach 1985). While recent observations and studies show that [C I] can coexist with CO deep inside molecular clouds, with a remarkably constant column density ratio between [C I] and CO (Ikeda et al. 2002). For nuclear regions or innermost disk centers of nearby galaxies, Israel (2005) found that the abundance of [C I] is close to, or even exceeds the CO abundance. Moreover, [C I] (1–0) and [C I] (2–1) emits 2 – 10 times higher energy than CO (1–0) (even in the coldest H₂ gas), so the [C I] lines are better tracers of cold molecular gas for high- z galaxies, comparing to the observed mid/high- J CO transitions which only pick up the dense and warm H₂ gas. In addition, recent studies shows that cosmic rays can destroy CO (but not H₂) very effectively, leaving behind a C-rich phase (e.g., Bisbas et al. 2015; Krips et al. 2016), which further indicates that the optically thin [C I] lines may represent a promising alternative to determine the total molecular gas.

Observations of [C I] emission in nearby galaxies have been difficult due to the fact that the atmospheric transmissions at these frequencies are poor, which severely

* Based on Herschel observations. Herschel is an ESA space observatory with science instruments provided by European-led Principal Investigator consortia and with important participation from NASA

¹ National Astronomical Observatories, Chinese Academy of Sciences (CAS), Beijing 100012, China; mz@nao.cas.cn

² Key Laboratory of Radio Astronomy, CAS, Beijing 100012, China

³ University of Chinese Academy of Sciences, Beijing 100012, China

⁴ Yunnan Observatories, CAS, Kunming 650011, China; zhaoyinghe@ynao.ac.cn

⁵ Key Laboratory for the Structure and Evolution of Celestial Objects, CAS, Kunming 650011, China

⁶ Center for Astronomical Mega-Science, CAS, 20A Datun Road, Chaoyang District, Beijing 100012, China

⁷ Purple Mountain Observatory, CAS, Nanjing 210008, China

⁸ China-Chile Joint Center for Astronomy (CCJCA), Camino El Observatorio 1515, Las Condes, Santiago, Chile; nanyao.lu@gmail.com

⁹ Key Laboratory of Radio Astronomy, CAS, Nanjing 210008, China

¹⁰ Institute for Astronomy, University of Edinburgh, Royal Observatory, Blackford Hill, Edinburgh EH9 3HJ, UK

¹¹ ESO, Karl Schwarzschild Strasse 2, D-85748 Garching, Munich, Germany

limits large surveys of the [C I] emission in the local Universe. However the limited observations of the [C I] emission using ground-based facilities in nearby (e.g., White et al. 1994; Ojha et al. 2001; Israel 2005) and high- z (Weiß et al. 2005, Walter et al. 2011) systems indeed suggest that [C I] may trace H_2 in galaxies near and far, similarly to the low- J CO lines (e.g., Zhang et al. 2014). Therefore it is important to have a large sample of local galaxies to carry out statistical studies and to compare to those of CO studies.

Thanks to the advent of the *Herschel Space Observatory* (*Herschel*; Pilbratt et al. 2010), a large number of local galaxies have been observed spectroscopically in the submillimeter window, using the *Herschel* Spectral and Photometric Imaging Receiver Fourier Transform Spectrometer (SPIRE/FTS; Griffin et al. 2010). Abundant ionized, atomic and molecular lines, including [C I] (1–0) and [C I] (2–1), are detected (e.g., Lu et al. 2017), which allows us to carry out robust statistical analysis.

In this letter, we present a statistical study on the [C I] (1–0) and [C I] (2–1) lines for a large sample of local luminous infrared galaxies (LIRGs; $L_{\text{IR}} \equiv L(8 - 1000 \mu\text{m}) > 10^{11} L_{\odot}$, Sanders et al. 2003) observed with the SPIRE/FTS. The remainder of the paper is organized as follows. We briefly introduce the sample, observations, and data reduction in Section 2. The results and discussion are presented in Section 3, where we investigate the correlation between the [C I] and CO (1–0) lines, and also calculate the conversion factors, $\alpha_{[\text{C I}]}$ ($\equiv M(H_2)/L'_{[\text{C I}]}$). In the last section we summarize the main conclusions. Throughout the letter, we use a Hubble constant of $H_0 = 70 \text{ km s}^{-1} \text{ Mpc}^{-1}$, $\Omega_M = 0.3$ and $\Omega_{\Lambda} = 0.7$.

2. SAMPLE AND DATA REDUCTION

The sample discussed in this letter is selected from the program *A Herschel Spectroscopic Survey of Warm Molecular Gas in Local LIRGs* (PI: N. Lu), which focuses on studying the dense and warm molecular gas properties of 125 LIRGs (e.g. Lu et al. 2014, 2015). These LIRGs comprise a flux-limited subset of the Great Observatories All-Sky LIRGs Survey sample (GOALS; Armus et al. 2009). The complete dataset of the spectral lines and their fluxes for individual galaxies is given in Lu et al. (2017), and the measured [C I] fluxes used here were based on the point-source flux calibration, as also described in Zhao et al. (2016) and Lu et al. (2014). Here we present a subsample of 71 galaxies (including 62 LIRGs and 9 ULIRGs with $L_{\text{IR}} > 10^{12} L_{\odot}$), which are selected based on the following two criteria:

1. A galaxy is point-like with respect to the *Herschel* SPIRE beam, which is $\sim 35''$ at 809 GHz ($\nu_{\text{rest}}^{[\text{C I}](2-1)}$). We used the Photodetector Array Camera and Spectrometer (PACS; Poglitsch et al. 2010) $70 \mu\text{m}$ continuum images of Chu et al. (2017) to select galaxies which are not too extended with respect to the SPIRE beam (Zhao et al. 2016, Lu et al. 2017). A galaxy is considered as a point source if its fractional $70 \mu\text{m}$ flux within a Gaussian beam of $35''$ is $> 80\%$, and we obtained 111 sources.

2. A galaxy which has CO (1–0) data (most from Sander et al. 1991; Young et al. 1995; Albrecht et al. 2007; Baan et al. 2008), with beam size greater than $35''$, which results in 71 sources. For the sources which

have multiple measurements, we adopted their average CO (1–0) fluxes, and used those having good signal-to-noise ratios for our calculations. The CO fluxes are shown in Table 1 and the [C I] fluxes can be found in Lu et al. (2017). All of these 71 sources have [C I] (2–1) detections, whereas only 23 have [C I] (1–0) detections due to the reduced sensitivity near the low-frequency end of the SPIRE Long Wavelength Spectrometer Array. Typical uncertainties of the CO (1–0), [C I] (1–0) and [C I] (2–1) line fluxes are 23% (calculated from different measurements in the literature), 13% and 8%, respectively, which already include the absolute calibration uncertainty of 6% for SPIRE FTS observations (Swinyard et al. 2014).

3. RESULTS AND DISCUSSION

3.1. Relations between [C I] and CO Emission

Figure 1 shows the correlations between $L'_{\text{CO}(1-0)}$, and $L'_{[\text{C I}](1-0)}$ (panel a) and $L'_{[\text{C I}](2-1)}$ (panel b), which are the luminosities of CO (1–0), [C I] (1–0) and [C I] (2–1), respectively. The filled (black) circles are the 23 galaxies with both [C I] (1–0) and [C I] (2–1) detected. The red (open) circles represent the other galaxies which have [C I] (2–1) detections (panel b) and [C I] (1–0) upper limits (panel a). These plots show that CO (1–0) is well correlated with both of the [C I] lines, with the corresponding correlation coefficients of 0.81 and 0.85 in panels (a) and (b), respectively. Unweighted least-squares linear fits, using a geometrical mean functional relationship (Isobe et al. 1990), to these 23 sources with both [C I] detections give:

$$\log L'_{\text{CO}(1-0)} = (-0.47 \pm 0.76) + (1.12 \pm 0.09) \log L'_{[\text{C I}](1-0)}, \quad (1)$$

and

$$\log L'_{\text{CO}(1-0)} = (0.56 \pm 1.55) + (1.07 \pm 0.19) \log L'_{[\text{C I}](2-1)}, \quad (2)$$

with vertical scatters of 0.18 and 0.21 dex, respectively. The fitted trends are shown in Figure 1 as dashed (black) lines. Furthermore, we obtain the following $L'_{\text{CO}(1-0)} - L'_{[\text{C I}](2-1)}$ relation for all of the 71 galaxies from a geometrical mean fitting:

$$\log L'_{\text{CO}(1-0)} = (1.46 \pm 0.69) + (0.97 \pm 0.08) \log L'_{[\text{C I}](2-1)}, \quad (3)$$

with a scatter of 0.19 dex. The fitted relation is overplotted in Figure 1b with solid (black) line. We also obtain the following $L'_{\text{CO}(1-0)} - L'_{[\text{C I}](1-0)}$ correlation (the solid black line in Figure 1a) using a Bayesian regression method (Kelly 2007) that also takes into consideration all the upper limits of [C I] (1–0):

$$\log L'_{\text{CO}(1-0)} = (-0.19 \pm 1.26) + (1.09 \pm 0.15) \log L'_{[\text{C I}](1-0)}, \quad (4)$$

Equations (1)-(4) suggest that the CO (1–0) emission likely has a linear correlation with the [C I] emission. For the [C I] (1–0) and [C I] (2–1) lines, the fitted slopes only have marginal differences, and are consistent with each other within 1σ . The nearly linear relations between

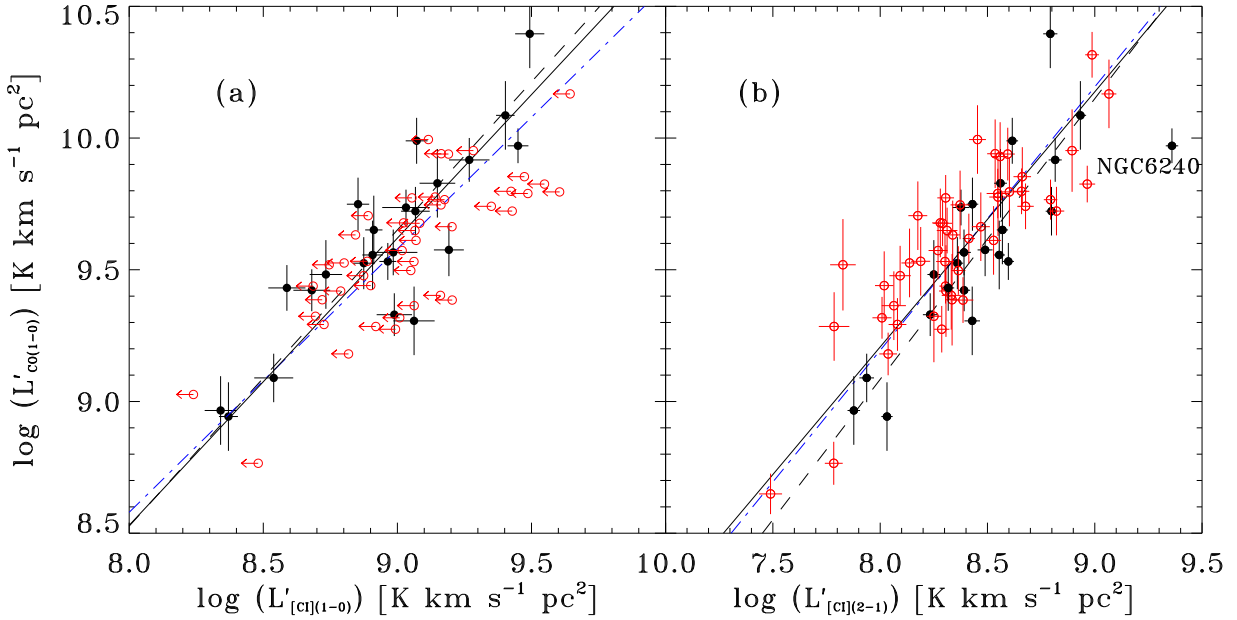


Figure 1. The luminosity of CO (1–0) is plotted against (a) [C I] (1–0) luminosity, and (b) [C I] (2–1) luminosity. The filled (black) circles represent the 23 galaxies having both [C I] (1–0) and [C I] (2–1) detections (panel b) and [C I] (1–0) upper limits (panel a). For the 23 galaxies, the best-fit relations with a free slope are shown by the dashed (black) lines. Whereas the best-fit relations with a fixed slope of 1 for each detected source are shown by the dash-dot (blue) lines. The solid (black) lines show the relations for all of the 71 galaxies. NGC 6240 in panel (b) is labelled due to its largest deviation from the relation.

$L'_{\text{CO}(1-0)}$ and $L'_{\text{[C I]}}$ indicate that the CO (1–0) and [C I] emissions might arise from similar regions within galaxies.

Considering that the low- J CO emission is a commonly used tracer of the total molecular gas, the [C I] (1–0) and [C I] (2–1) lines thus can be a new avenue to determine the total molecular gas at least in (U)LIRGs. This might be particularly useful for measuring the total molecular gas mass in high- z galaxies since their CO (1–0) lines are difficult to observe using ground-based facilities, whereas the [C I] lines from distant sources become accessible for ground mm/submm telescopes.

Given such a strong (and almost linear) correlation, we also fitted the $L'_{\text{CO}(1-0)} - L'_{\text{[C I]}}$ relations with a fixed slope of 1 in order to reduce any systemic uncertainties caused by the sample itself (e.g., sample size, dynamic range, etc.), resulting in:

$$\log L'_{\text{CO}(1-0)} = (0.65 \pm 0.02) + \log L'_{\text{[C I]}(1-0)}, \quad (5)$$

with a scatter of 0.17 dex, and

$$\log L'_{\text{CO}(1-0)} = (1.19 \pm 0.01) + \log L'_{\text{[C I]}(2-1)}, \quad (6)$$

with a scatter of 0.19 dex. The fitted relations are also plotted in Figure 1 with dash-dot (blue) lines. If we adopt the CO conversion factor $\alpha_{\text{CO}} \equiv M(\text{H}_2)_{\text{CO}}/L'_{\text{CO}(1-0)} = 0.8 M_{\odot} (\text{K km s}^{-1} \text{pc}^2)^{-1}$ (Downes & Solomon 1998), we can obtain the [C I] conversion factors $\alpha_{\text{[C I],CO}}$, i.e., $\alpha_{\text{[C I]}(1-0),\text{CO}} = 3.6 \pm 0.2 M_{\odot} (\text{K km s}^{-1} \text{pc}^2)^{-1}$ and $\alpha_{\text{[C I]}(2-1),\text{CO}} = 12.5 \pm 0.3 M_{\odot} (\text{K km s}^{-1} \text{pc}^2)^{-1}$, respectively. Here we only considered the fitted errors of the intercepts. A more practical choice is to take the scatters in the fitted relations as the final uncertainties, e.g., a factor of ~ 1.5 .

The galaxy with the largest deviation in Figure 1b is

NGC 6240, in which the gas heating is likely dominated by shocks (Meijerink et al. 2012). As shown in Figure 2a, NGC 6240 has the highest excitation temperature in the sample. Therefore, the temperature influence on the level populations of C I in NGC 6240 is likely the highest in this sample.

In Figure 2, we show the luminosity ratios of $L'_{\text{[C I]}(1-0)}/L'_{\text{CO}(1-0)}$ and $L'_{\text{[C I]}(2-1)}/L'_{\text{CO}(1-0)}$, as well as the [C I] line ratio: $L'_{\text{[C I]}(2-1)}/L'_{\text{[C I]}(1-0)}$ (hereafter $R_{\text{[C I]}}$) as a function of the IRAS $60 \mu\text{m}/100 \mu\text{m}$ color (f_{60}/f_{100}) for our sample. We check possible correlations in these plots using the *cenreg* function in NADA package within the \mathbf{R}^{11} statistical software environment. As labelled in panels (a) and (b) of Figures 2, the likelihood- r coefficients are 0.11 and 0.33, respectively, with the possibilities of having no correlation at 0.36 and 5.4×10^{-3} , respectively. Therefore, we conclude that there is no correlation between $L'_{\text{[C I]}(1-0)}/L'_{\text{CO}(1-0)}$ and f_{60}/f_{100} (Figure 2a). Whereas $L'_{\text{[C I]}(2-1)}/L'_{\text{CO}(1-0)}$ shows a weak correlation with f_{60}/f_{100} (Figure 2b), with a monotone increasing trend. Figure 2c shows that $R_{\text{[C I]}}$ is modestly correlated with f_{60}/f_{100} .

The observed weak correlations involving the [C I] (2–1) line might be due to the relatively higher energy required for exciting [C I] (2–1), comparing to that of [C I] (1–0) and CO (1–0). [C I] (2–1) is sensitive to high gas temperature, which also correlates to f_{60}/f_{100} as an indicator of the intensity of the ambient UV field (thus the gas temperature, e.g. Abel et al. 2009). As shown in next subsection, the excitation temperatures of our sample galaxies are typically in the range 20–30 K, which is very close to the excitation energy of [C I] (1–0) (24 K), but significantly lower than

¹¹ <http://www.R-project.org/>

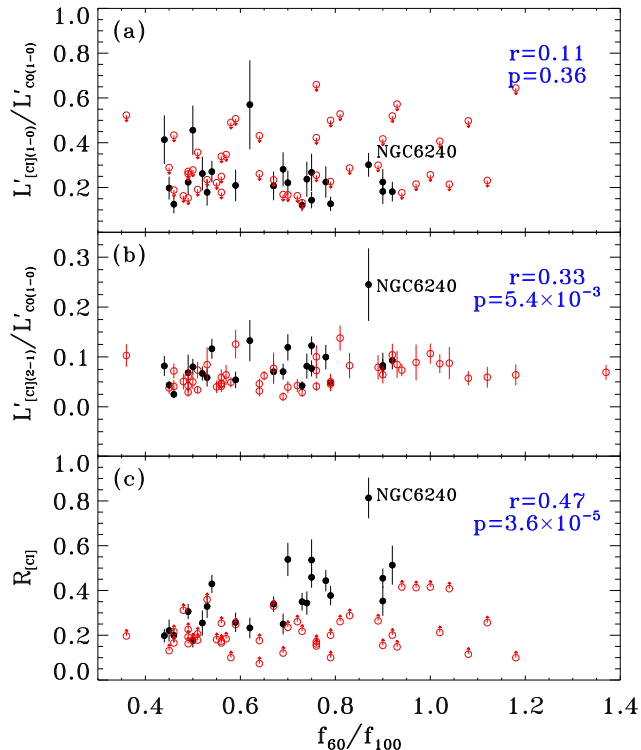


Figure 2. Plots of (a) $L'_{[\text{C I}](1-0)}/L'_{\text{CO}(1-0)}$, (b) $L'_{[\text{C I}](2-1)}/L'_{\text{CO}(1-0)}$, and (c) $R_{[\text{C I}]}$ against f_{60}/f_{100} . The open (red) circles in panels a (c) indicate the upper (lower) limits. The Labelled r and p represent the correlation coefficient and the possibility of no correlation respectively.

the excitation energy of $[\text{C I}](2-1)$ (63 K). Thus the $[\text{C I}](2-1)$ is more sensitive to temperature.

3.2. Total Molecular Gas Mass

The nearly linear luminosity correlations between the $[\text{C I}]$ lines and $\text{CO}(1-0)$ suggest that either $[\text{C I}]$ line can substitute $\text{CO}(1-0)$ as a tracer of the total molecular gas mass. In this subsection, we further calculate the total molecular gas mass directly from the observed $[\text{C I}]$ line fluxes to derive a carbon conversion factor $\alpha_{[\text{C I}]}$, and check whether $\alpha_{[\text{C I}]}$ agrees with $\alpha_{[\text{C I}],\text{CO}}$. Here we also include those 7 galaxies that are detected in both $[\text{C I}]$ lines, but lack $\text{CO}(1-0)$ data.

To derive the total molecular gas mass, we adopt the equation given by Papadopoulos et al. (2004) assuming optically thin $[\text{C I}]$ emission:

$$M(\text{H}_2)_{[\text{C I}]} = \frac{4\pi m_{\text{H}_2}}{hc A_{\text{ul}} X_{[\text{C I}]}} \left(\frac{D_L^2}{1+z} \right) Q_{\text{ul}}^{-1} I_{[\text{C I}]}, \quad (7)$$

where $Q_{\text{ul}} = N_{\text{u}}/N_{[\text{C I}]}$ is the excitation factor which depends on the gas temperature (T_{kin}) and density (n) (Papadopoulos et al. 2004), and on the radiation field, A_{ul} the Einstein coefficient, with $A_{10} = 7.93 \times 10^{-8} \text{ s}^{-1}$ and $A_{21} = 2.68 \times 10^{-7} \text{ s}^{-1}$, $X_{[\text{C I}]}$ the abundance ratio of C I to H_2 , and here we adopt 3×10^{-5} (Weiß et al. 2003), z the redshift, and D_L the luminosity distance.

The line ratio $R_{[\text{C I}]}$ can be used to estimate the excitation temperature by adopting the equation $T_{\text{ex}} = 38.8 \text{ K}/\ln[2.11/R_{[\text{C I}]}]$ (Stutzki et al. 1997). For those

30 galaxies having both $[\text{C I}]$ lines detected, their T_{ex} are given in Table 2. The table shows that the excitation temperatures of most sources in our sample are in the range of 20 – 30 K. To calculate Q_{ul} , we used equations A21 and A22 in Papadopoulos et al. (2004) to avoid assuming local thermodynamic equilibrium (LTE). These equations are derived assuming an optically thin case and using the weak radiation field approximation, i.e., $T_{\text{kin}} \gg T_{\text{CMB}} \sim 2.7 \text{ K}$, where T_{CMB} is the temperature of the cosmic microwave background. We also simply set T_{ex} as T_{kin} since it is difficult to have an accurate T_{kin} and T_{ex} might not deviate much from T_{kin} for our sample galaxies. Then at each T_{ex} , we computed Q_{ul} for four gas densities of 10^3 , 3×10^3 , 5×10^3 , 10^4 cm^{-3} according to Papadopoulos & Greve (2004), and adopted the averaged value as the final Q_{ul} . However, we find that $Q_{10}/Q_{10}^{(\text{LTE})} \sim 0.94$ and $Q_{21}/Q_{21}^{(\text{LTE})} \sim 0.76$, where $Q_{\text{ul}}^{(\text{LTE})}$ were calculated in LTE using the same assumed T_{kin} , indicating that our adopted physical parameters are very close to an LTE condition. The derived masses of carbon, and H_2 are also listed in Table 2.

In the top panels of Figure 3, we plot the resulting $M(\text{H}_2)$ as a function of $L'_{[\text{C I}]}$. The red and olive lines in each plot show the two cases with $(n, T_{\text{kin}}) = (10^3 \text{ cm}^{-3}, 20 \text{ K})$ and $(10^4 \text{ cm}^{-3}, 30 \text{ K})$, respectively. The dashed (black) lines are unweighted least-squares fits to these data points, which give:

$$\log M(\text{H}_2)_{[\text{C I}](1-0)} = (0.63 \pm 0.19) + (1.02 \pm 0.02) \log L'_{[\text{C I}](1-0)}, \quad (8)$$

and

$$\log M(\text{H}_2)_{[\text{C I}](2-1)} = (1.78 \pm 1.00) + (0.96 \pm 0.13) \log L'_{[\text{C I}](2-1)}, \quad (9)$$

with scatters of 0.04 dex and 0.24 dex, respectively. We also fit these models using a fixed slope of 1, and obtained:

$$\log M(\text{H}_2)_{[\text{C I}](1-0)} = (0.88 \pm 0.01) + \log L'_{[\text{C I}](1-0)}, \quad (10)$$

and

$$\log M(\text{H}_2)_{[\text{C I}](2-1)} = (1.44 \pm 0.02) + \log L'_{[\text{C I}](2-1)}, \quad (11)$$

with scatters of 0.05 dex and 0.24 dex. The fitted results are plotted in Figure 3 as dash-dotted (blue) lines.

As shown in Figures 3a and b, the derived model of $M(\text{H}_2)_{[\text{C I}](1-0)}$ from $L'_{[\text{C I}](1-0)}$ shows a smaller dispersion than that of $M(\text{H}_2)_{[\text{C I}](2-1)}$ from $L'_{[\text{C I}](2-1)}$. This is because Q_{21} is much more sensitive to temperature and density than Q_{10} , which is illustrated clearly in Figures 3c and d. Hence, the $[\text{C I}](1-0)$ emission is a better total molecular gas mass tracer compared to the $[\text{C I}](2-1)$ line in the theoretical aspect if we do not have constrains on the gas temperature and density. However, in practice the variation of the C I abundance (see below) and/or violation of the assumption of optically thin $[\text{C I}]$ emission may wash out this effect and result in similar scatter for both lines as indicated in Figure 1.

We calculated the conversion factors using equations (10) and (11), and obtained $\alpha_{[\text{C I}](1-0)} = 7.6 \pm 0.2 (\text{K km s}^{-1} \text{ pc}^2)^{-1}$ and $\alpha_{[\text{C I}](2-1)} = 27.5 \pm 1.3 (\text{K km s}^{-1} \text{ pc}^2)^{-1}$. These values are about 2 times larger than those (see §3.1) derived from the $[\text{C I}]$ – CO

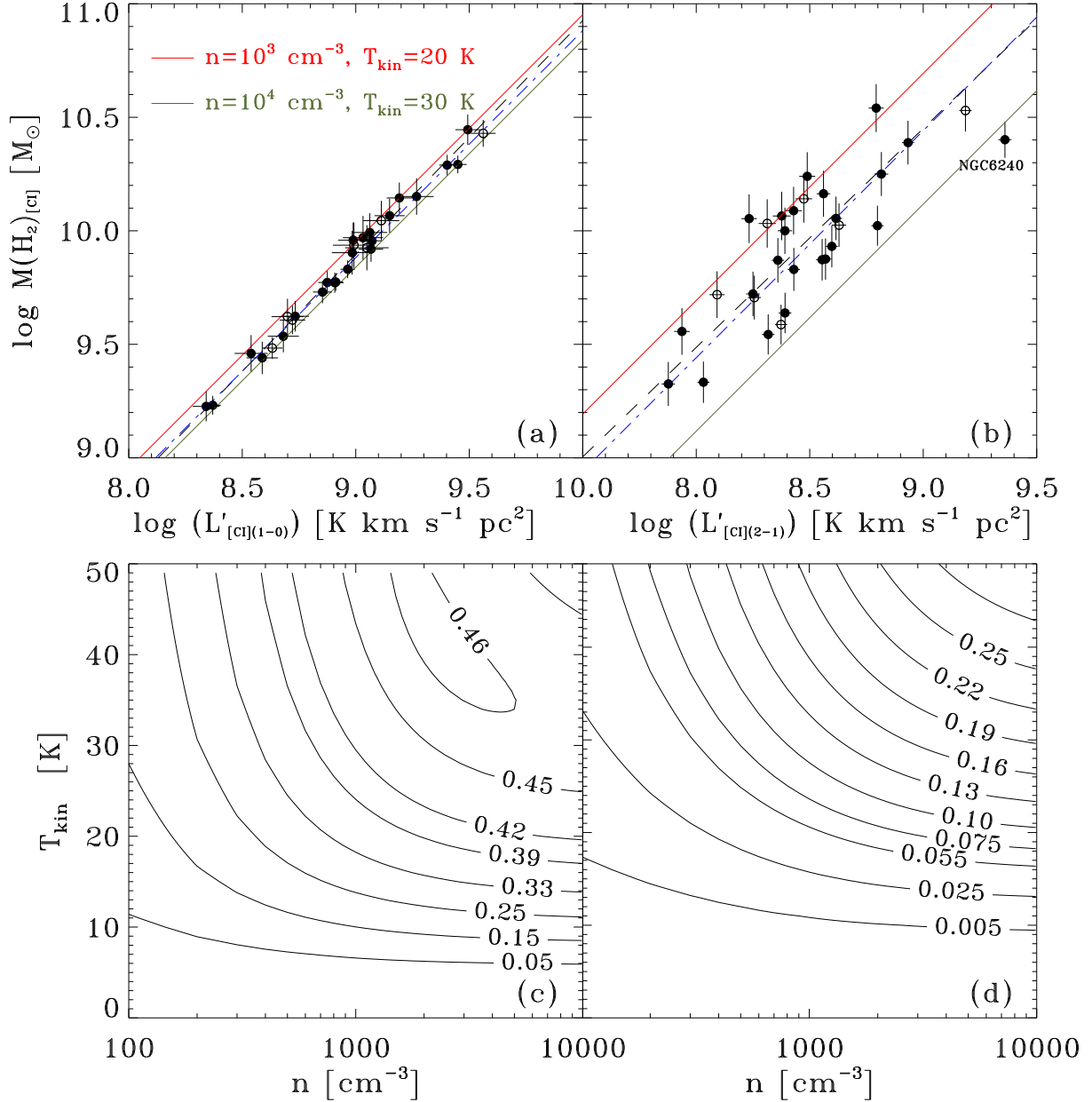


Figure 3. Panels (a) and (b) are H₂ masses calculated from the [C I] (1–0) and [C I] (2–1) emission plotted against [C I] (1–0) and [C I] (2–1) luminosities, respectively. Panels (c) and (d) show the Q_{10} and Q_{21} contours as a function of gas temperature (T_{kin}) and density (n), respectively. In the top panels, the filled and open circles are galaxies with/without CO (1–0) data. The best-fit models with a fixed slope of 1 are shown by the dashed dot (blue) lines, whereas the best-fit models with a free slope are shown by the dashed (black) lines. The red and olive lines indicate the two cases with density of 10^3 cm^{-3} and temperature of 20 K, and density of 10^4 cm^{-3} and temperature of 30 K, respectively.

relations with $\alpha_{\text{CO}} = 0.8 (\text{K km s}^{-1} \text{ pc}^2)^{-1}$. Several reasons could cause these discrepancies: (1) the adopted α_{CO} is smaller than its real value; (2) our adopted $X_{[\text{C I}]}$ is too high; and/or (3) the density we adopted to calculate Q_{ul} is too low. Indeed, Papadopoulos et al. (2012) and Scoville et al. (2016) found that even in (U)LIRGs α_{CO} can be as high as the Galactic value. Regarding $X_{[\text{C I}]}$, several studies on local and high-redshift star-forming environments have shown that it is in the range of $2 - 16 \times 10^{-5}$ (Pety et al. 2004; Weiß et al. 2005; Walter et al. 2011). Further, Q_{ul} varies by a factor of 1–2 when the density changing from 10^3 to 10^4 cm^{-3} within our temperature range. Therefore, all of these

uncertainties make our estimators have accuracies of a factor of 2–3.

4. SUMMARY

In this letter, we present the relations of the [C I] (1–0), [C I] (2–1) lines with the CO (1–0) line for a sample of 71 (U)LIRGs which were observed with the Herschel SPIRE/FTS. We investigate the dependence of $L'_{[\text{C I}](2-1)}/L'_{\text{CO}(1-0)}$, $L'_{[\text{C I}](1-0)}/L'_{\text{CO}(1-0)}$ and the [C I] intensity ratio $R_{[\text{C I}]}$ on far-infrared color (f_{60}/f_{100}). We also calculate the conversion factors of $\alpha_{[\text{C I}](1-0)}$ and $\alpha_{[\text{C I}](2-1)}$, based on the assumption that the carbon is optically thin, and on the [C I]–CO relation. Our main

Table 1
The CO(1–0) flux

galaxy ^a	$I_{\text{CO}(1-0)}$ Jy km s ⁻¹	Ref. ^b	galaxy	$I_{\text{CO}(1-0)}$ Jy km s ⁻¹	Ref. ^b
Arp 193 *	182.6 ± 38.8	B08, P12	ESO 069-IG006	197.1 ± 39.4	M90
Arp 220 *	445.3 ± 85.3	Y95, B08, P12	ESO 148-IG002	59.4 ± 11.9	M90
CGCG 049-057 *	119.1 ± 25.3	B08, P12	ESO 244-G012	170.1 ± 51.0	A07
ESO 320-G030 *	225.3 ± 67.6	B08	ESO 255-IG007	89.1 ± 17.8	M90
IRASF 18293-3413 *	686.1 ± 205.8	B08	ESO 286-IG019	71.5 ± 21.5	G99
Mrk 331 *	371.2 ± 86.2	Y95, S91	ESO 467-G027	191.7 ± 57.5	A07
NGC 3256 *	1222.8 ± 366.8	B08	ESO 507-G070	152.0 ± 45.6	P12
NGC 5135 *	380.4 ± 61.4	S91, B08, P12	IC 4280	310.5 ± 93.2	A07
NGC 6240 *	290.9 ± 44.3	Y95, S91, B08, P12	IC 4734	367.2 ± 110.2	G93
NGC 7469 *	298.0 ± 89.4	P12	IC 5298	72.0 ± 14.4	S91
NGC 7552 *	652.0 ± 195.6	B08	IRASF 01417+1651	75.0 ± 22.5	G99
NGC 7771 *	370.3 ± 84.2	Y95, S91	IRASF 10565+2448	73.5 ± 11.8	S91, B08, P12
NGC 6286 *	213.3 ± 49.0	Y95, S91	IRASF 16399-0937	118.1 ± 35.4	B08
CGCG 052-037 *	63.0 ± 18.9	P12	MCG-03-04-014	178.0 ± 53.4	P12
NGC 0828 *	389.3 ± 60.8	Y95, S91, B08, P12	NGC 0023	203.0 ± 37.1	S91, Y95, A07
NGC 2369 *	553.8 ± 166.4	B08	NGC 0317	180.6 ± 72.4	Z99
NGC 6701 *	227.2 ± 42.5	Y95, P12, S91	NGC 0695	190.0 ± 43.8	Y95, S91
UGC 02238 *	180.0 ± 36.0	S91	NGC 1275	180.0 ± 72.0	L89
VV 340 *	426.6 ± 128.0	G99	NGC 3110	390.0 ± 78.0	S91
NGC 2623 *	155.8 ± 28.6	S91, Y95, P12	NGC 4194	129.9 ± 24.5	S91, A07, Y95
MCG+12-02-001 *	230.0 ± 46.0	G12	NGC 5104	158.7 ± 33.7	A07, P12
IC 1623 *	557.0 ± 111.9	S91, P12	NGC 5653	173.0 ± 32.2	S91, P12
NGC 0232 *	310.5 ± 93.2	A95	NGC 5936	180.4 ± 41.6	Y95, S91
IRASF 05189-2524	72.8 ± 24.8	S91, B08, P12	NGC 5990	299.8 ± 78.2	A07, P12
IRASF 17207-0014	160.0 ± 48.0	P12	NGC 6621	159.5 ± 41.1	S91, Z99
Mrk 231	103.6 ± 37.4	Y95, B08, A07, P12	NGC 7591	171.7 ± 68.7	L98
Mrk 273	82.8 ± 14.5	S91, B08, P12	NGC 7592	177.0 ± 35.4	S91
NGC 1614	247.7 ± 37.8	Y95, B08, A07, S91	NGC 7674	120.0 ± 24.0	S91
NGC 7130	326.7 ± 70.9	B08, A07	NGC 7679	252.3 ± 100.9	W89
UGC 05101	71.7 ± 15.2	B08, P12	UGC 02608	413.1 ± 123.9	A07
CGCG 448-020	100.7 ± 27.8	B08, P12	UGC 02982	277.5 ± 70.1	Y95, A07
UGC 03094	207.9 ± 62.4	A07	IRAS 05442+1732	148.5 ± 44.6	A07
UGC 03351	411.1 ± 123.3	B08	NGC 4418	137.85 ± 24.5	Y95, B08, S91, P12
UGC 08739	118.0 ± 24.0	P12	NGC 6052	132.8 ± 39.9	A07
UGC 11041	232.2 ± 69.7	A07	UGC 02369	194.0 ± 58.2	G99
VV 705	90.6 ± 23.4	A07, P12			

Note. — ^(a) The symbols “*” represent the 23 galaxies which have [C I](1–0) detections.

Note. — ^(b) Reference to CO(1–0) data: B08 = Baan et al. 2008, P12 = Papadopoulos et al. 2012, Y95 = Young et al. 1995, S91 = Sanders et al. 1991, G99 = Gao & Solomon 1999, G12 = García-Burillo et al. 2012, A95 = Andreani et al. 1995, A07 = Albrecht et al. 2007, M90 = Mirabel et al. 1990, G93 = Garay et al. 1993, Z99 = Zhu et al. 1999, L98 = Lavezzi et al. 1998, W89 = Wiklind & Henkel 1989.

results are as follows:

1. There is an obvious correlation between $L'_{[\text{C I}](1-0)}$ and $L'_{\text{CO}(1-0)}$ in (U)LIRGs, i.e., $\log L'_{\text{CO}(1-0)} = (-0.23 \pm 1.32) + (1.10 \pm 0.15) \log L'_{[\text{C I}](1-0)}$. $L'_{[\text{C I}](2-1)}$ also correlates well with $L'_{\text{CO}(1-0)}$, namely, $\log L'_{\text{CO}(1-0)} = 1.46 \pm 0.69 + (0.97 \pm 0.08) \log L'_{[\text{C I}](2-1)}$. These results imply that the [C I](1–0), [C I](2–1) lines can be used as total molecular tracers at least for (U)LIRGs.

2. We find that $L'_{[\text{C I}](2-1)}/L'_{\text{CO}(1-0)}$ depends weakly on f_{60}/f_{100} , while $L'_{[\text{C I}](1-0)}/L'_{\text{CO}(1-0)}$ has no correlation

with f_{60}/f_{100} .

3. Based on the [C I]–CO relations, we derive the conversion factors of $\alpha_{[\text{C I}](1-0), \text{CO}} = 3.6$ and $\alpha_{[\text{C I}](2-1), \text{CO}} = 12.5 (\text{K km s}^{-1} \text{pc}^2)^{-1}$. Whereas the conversion factors derived from a more direct method are $\alpha_{[\text{C I}](1-0)} = 7.6$ and $\alpha_{[\text{C I}](2-1)} = 27.5 (\text{K km s}^{-1} \text{pc}^2)^{-1}$ by assuming a constant [C I] abundance. The accuracy is about a factor of 2–3.

The authors thank the referee for useful suggestions. This work is partially supported by the Natural Science Foundation of China under grant NOs. 11673057, U1531246, 11420101002, 11673028 and 11311130491.

Table 2
Physical parameters of the sample

galaxy	$R_{[\text{C I}]}$	Tex (K)	$M_{[\text{C I}]}$ ^a ($10^6 M_{\odot}$)	$M(\text{H}_2)_{\text{CO}}$ ($10^9 M_{\odot}$)	$M(\text{H}_2)_{[\text{C I}](1-0)}$ ($10^9 M_{\odot}$)	$M(\text{H}_2)_{[\text{C I}](2-1)}$ ($10^9 M_{\odot}$)
Arp 193	0.54 ± 0.07	28.4 ± 2.9	1.5 ± 0.2	4.3 ± 0.9	8.3 ± 1.1	10.5 ± 2.2
Arp 220	0.35 ± 0.07	21.7 ± 2.3	2.5 ± 0.5	6.6 ± 1.3	14.2 ± 2.6	17.8 ± 4.0
CGCG 049-057	0.25 ± 0.05	18.2 ± 1.6	0.5 ± 0.1	1.0 ± 0.2	2.9 ± 0.6	3.6 ± 0.9
ESO 320-G030	0.34 ± 0.05	21.4 ± 1.8	0.3 ± 0.05	0.8 ± 0.2	1.7 ± 0.3	2.1 ± 0.5
IRASF 18293-3413	0.34 ± 0.03	21.3 ± 1.2	3.5 ± 0.4	9.8 ± 3.0	19.5 ± 2.0	24.4 ± 5.5
Mrk 331	0.38 ± 0.04	22.6 ± 1.5	1.0 ± 0.1	4.5 ± 1.1	5.4 ± 0.6	6.8 ± 1.5
NGC 3256	0.45 ± 0.04	25.3 ± 1.6	1.1 ± 0.1	3.6 ± 1.1	5.9 ± 0.5	7.5 ± 1.6
NGC 5135	0.43 ± 0.04	24.4 ± 1.5	1.2 ± 0.1	2.8 ± 0.4	6.8 ± 0.6	8.5 ± 1.9
NGC 6240	0.81 ± 0.09	40.7 ± 4.8	3.5 ± 0.3	7.5 ± 1.2	19.6 ± 1.8	25.2 ± 4.6
NGC 7469	0.44 ± 0.05	24.9 ± 1.7	1.1 ± 0.1	2.9 ± 0.9	5.9 ± 0.6	7.5 ± 1.6
NGC 7552	0.46 ± 0.05	25.5 ± 1.7	0.3 ± 0.03	0.7 ± 0.2	1.7 ± 0.2	2.2 ± 0.5
NGC 7771	0.31 ± 0.03	20.1 ± 1.2	1.1 ± 0.1	2.7 ± 0.6	5.9 ± 0.7	7.4 ± 1.7
NGC 6286	0.20 ± 0.03	16.5 ± 1.1	2.5 ± 0.4	3.0 ± 0.7	14.0 ± 2.2	17.4 ± 4.3
CGCG 052-037	0.23 ± 0.05	17.7 ± 1.5	1.8 ± 0.3	1.6 ± 0.5	9.8 ± 2.0	12.3 ± 3.0
NGC 0828	0.23 ± 0.05	17.2 ± 1.7	1.7 ± 0.4	4.4 ± 0.7	9.3 ± 2.1	11.6 ± 2.9
NGC 2369	0.33 ± 0.05	20.9 ± 1.7	0.8 ± 0.1	2.5 ± 0.7	4.2 ± 0.7	5.3 ± 1.2
NGC 6701	0.18 ± 0.03	15.6 ± 1.1	1.6 ± 0.3	1.8 ± 0.3	9.1 ± 1.6	11.3 ± 2.8
UGC 02238	0.25 ± 0.06	18.4 ± 1.9	1.4 ± 0.3	3.0 ± 0.6	8.0 ± 1.8	10.0 ± 2.4
VV 340	0.20 ± 0.03	16.5 ± 1.0	5.0 ± 0.8	19.9 ± 6.0	27.9 ± 4.3	34.7 ± 8.5
NGC 2623	0.51 ± 0.09	27.5 ± 3.3	0.6 ± 0.1	2.1 ± 0.4	3.4 ± 0.6	4.3 ± 0.9
MCG+12-02-001	0.54 ± 0.09	28.4 ± 3.6	0.5 ± 0.08	2.2 ± 0.4	2.8 ± 0.5	3.5 ± 0.7
IC 1623	0.35 ± 0.04	21.6 ± 1.4	1.6 ± 0.2	7.8 ± 1.6	9.0 ± 1.0	11.3 ± 2.5
NGC 0232	0.26 ± 0.04	18.5 ± 1.5	2.1 ± 0.4	5.4 ± 1.6	11.7 ± 2.0	14.6 ± 3.4
ESO 264-G036	0.23 ± 0.05	17.5 ± 1.6	2.0 ± 0.4		11.1 ± 2.2	13.8 ± 3.3
IRAS 12116-5615	0.38 ± 0.09	22.6 ± 3.1	1.5 ± 0.3		8.4 ± 2.0	10.6 ± 2.3
UGC 12150	0.21 ± 0.05	16.8 ± 1.7	1.6 ± 0.4		8.6 ± 2.0	10.8 ± 2.6
IRAS 13120-5453	0.42 ± 0.06	24.1 ± 2.1	4.8 ± 0.7		26.9 ± 3.7	33.9 ± 7.2
ESO 173-G015	0.55 ± 0.07	28.9 ± 2.6	0.5 ± 0.06		3.0 ± 0.3	3.9 ± 0.8
IC 4687	0.34 ± 0.05	21.4 ± 1.7	0.7 ± 0.1		4.0 ± 0.6	5.1 ± 1.1
NGC 0034	0.25 ± 0.04	18.1 ± 1.5	0.8 ± 0.1		4.2 ± 0.8	5.2 ± 1.3

Note. — ^(a) The carbon mass $M_{[\text{C I}]} = 6 \times M(\text{H}_2)X_{[\text{C I}]}$, is calculated using the [C I] (1–0) line.

Note. — Column 2 is the line ratio of [C I] (2–1) to [C I] (1–0); column 3 is the excitation temperature derived with the [C I] lines; column 4 is the carbon mass calculated from [C I] (1–0); column 5 is the H₂ gas mass calculated from the CO (1–0) line; columns 6 and 7 are the H₂ gas mass calculated from the [C I] (1–0) and [C I] (2–1) lines.

YG thanks partial support of the CAS Key Research Program of Frontier Sciences. Z-Y.Z. acknowledges support from ERC in the form of the Advanced Investigator Programme, 321302, COSMICISM.

REFERENCES

- Abel, N. P., Dudley, C., Fischer, J., Satyapal, S., & van Hoof, P. A. M. 2009, *ApJ*, 701, 1147
- Albrecht, M., Krgel, E., & Chini, R., 2007, *A&A*, 462, 575
- Andreani, P., Casoli, F., & Gerin, M. 1995, *A&A*, 300, 43
- Armus, L., Mazzarella, J. M., Evans, A. S., et al. 2009, *PASP*, 121, 559
- Baan, W. A., Henkel, C., Loenen, A. F., Baudry, A., & Wiklind, T. 2008, *A&A*, 477, 747
- Bisbas, T. G., Papadopoulos, P. P., & Viti, S. 2015, *ApJ*, 803, 37
- Bolatto, A. D., Wolfire, M., & Leroy, A. K. 2013, *ARA&A*, 51, 207
- Carilli, C. L., & Walter, F., 2013, *ARA&A*, 51, 105
- Chu, Jason K., Sanders, D. B., Larson, K. L., et al. 2017, *ApJS*, 229, 25
- Downes, D., & Solomon, P. M. 1998, *ApJ*, 507, 615
- García-Burillo, S., Usero, A., Alonso-Herrero, A., et al. 2012, *A&A*, 539, A8
- Garay, G., Mardones, D., & Mirabel, I. F. 1993, *A&A*, 277, 405
- Gao, Y., & Solomon, P. M., 1999, *ApJ*, 512, L99
- Griffin, M. J., Abergel, A., Abreu, A., et al. 2010, *A&A*, 518, L3
- Israel, F.P., 2005, *Ap&SS*, 295, 171
- Isobe, T., Feigelson, E. D., Akritas, M. G., & Babu, G. J. 1990, *ApJ*, 364, 104
- Ikedo, M., Oka, T., Tatematsu, K., Sekimoto, Y., & Yamamoto, S. 2002, *ApJS*, 139, 467
- Kelly, B. C. 2007, *ApJ*, 665, 1489
- Krips, M., Martín, S., Sakamoto, K., et al. 2016, *A&A*, 592, L3
- Lavezzi, T. E., & Dickey, J. M. 1998, *AJ*, 115, 405
- Lu, N., Zhao, Y., Xu, C. K., et al. 2014, *ApJL*, 787, L23
- Lu, N., Zhao, Y., Xu, C. K., et al. 2015, *ApJL*, 802, L11
- Lu, N., Zhao, Y., Díaz-Santos, T., et al. 2017, *ApJS* (arXiv:1703.00005)
- Meijerink, R., Kristensen, L. E., Weiß, A., et al. 2012, *ApJ*, 762, L16
- Mirabel, I. F., Booth, R. S., Johansson, L. E. B., et al. 1990, *A&A*, 236, 327
- Ojha, R., Stark, A. A., Hsieh, H. H., et al. 2001, *ApJ*, 548, 253
- Papadopoulos, P. P., Thi, W.-F., & Viti, S., 2004, *MNRAS*, 351, 147
- Papadopoulos, P. P., & Greve, T. R., 2004, *ApJ*, 615, L29
- Papadopoulos, P. P., van der Werf, P. P., & Xilouris, E. M., 2012, *MNRAS*, 426, 2601
- Pety, J., Beelen, A., Cox, P., et al. 2004, *A&A*, 428, L21

- Pilbratt, G. L., Riedinger, J. R., Passvogel, T., et al. 2010, *A&A*, 518, L1
- Poglitsch, A., Waelkens, C., Geis, N., et al. 2010, *A&A*, 518, L2
- Sanders, D. B., Scoville, N. Z., & Soifer, B. T. 1991, *ApJ*, 370, 158
- Sanders, D. B., Mazzarella, J. M., Kim, D.-C., Surace, J. A., & Soifer, B. T. 2003, *AJ*, 126, 1607
- Scoville, N., Sheth, K., Aussel, H., et al. 2016, *ApJ*, 820, 83
- Solomon, P. M., & Vanden Bout, P. A. 2005, *ARA&A*, 43, 677
- Stutzki, J., Graf, U. U., & Haas, S., 1997, *ApJ*, 477, L33
- Swinyard, B. M., Polehampton, E. T., Hopwood, R., et al. 2014, *MNRAS*, 440, 3658
- Tielens, A. G. G. M., & Hollenbach, D., 1985, *ApJ*, 291, 722
- Walter, F., Weiß, A., Downes, D., Decarli, R., & Henkel, C., 2011, *ApJ*, 730, 18
- Weiß, A., Downes, D., Henkel, C., & Walter, F., 2005, *A&A*, 409, L23
- Weiß, A., Henkel, C., Downes, D., & Walter, F., 2003, *A&A*, 429, L41
- White, G. J., Ellison, B., Claude, S., et al. 1994, *A&A*, 284, 23
- Wiklind, T., & Henkel, C., 1989, *A&A*, 225, 1
- Yang, B., Stancil, P. C., Balakrishnan, N., & Forrey, R. C. 2010, *ApJ*, 718, 1062
- Young, J. S., Xie, S., Tacconi, L., et al. 1995, *ApJS*, 98, 219
- Zhao, Y., Lu, N., Xu, C. K., et al. 2016, *ApJ*, 819, 69
- Zhang, Z.-Y., Henkel, C., Gao, Y., et al. 2014, *A&A*, 568, A122
- Zhang, Z.-Y., Papadopoulos, P. P., Ivison, R. J., et al. 2016, *Royal Society Open Science*, 3, 6
- Zhu, M., Seaquist, E. R., Davoust, E., et al. 1999, *AJ*, 118, 145